JPE 17-4-4

https://doi.org/10.6113/JPE.2017.17.4.884
ISSN(Print): 1598-2092 / ISSN(Online): 2093-4718

# Improved Transfer Functions for Modified Sheppard-Taylor Converter that Operates in CCM: Modeling and Application

Faqiang Wang†

†State Key Laboratory of Electrical Insulation and Power Equipment, School of Electrical Engineering, Xi'an Jiaotong University, Xi'an, China

**Abstract**

The improved transfer functions of the modified Sheppard–Taylor (MS-T) converter, which is capable of regulating output voltage under a wide range of input voltage and load variations, negligible current ripple, and fewer components in comparison to the Sheppard–Taylor (S-T) converter, operating in continuous conduction mode (CCM) are investigated in this study. Its DC equilibrium point, small signal model, and transfer functions are derived and analyzed. Then, the voltage controller is applied for this MS-T converter. The comparisons between the derived model and the existing model are presented. The hardware circuit is designed and the circuit experiments are provided for validation. The results show that the improved transfer functions of the MS-T converter are more effective and general than the previous ones for describing its real characteristics.

**Key words:** Modified Sheppard–Taylor (MS-T) converter, Stability, Transfer functions, Voltage controller

## I. INTRODUCTION

In recent years, to obtain the high output voltage to satisfy the increasing requirements in practical applications, many effective topologies of boosting voltage DC-DC converters have been proposed [1]-[7], such as Boost converter, Cuk converter, Sepic converter, Zeta converter, Luo converter, KY converter, and Sheppard–Taylor (S-T) converter. In 2011, Hua, Chiang, and Li [8] developed a new topology called modified Sheppard–Taylor (MS-T) converter to boost the voltage DC-DC converter by removing certain components of the S-T converter. Compared to other boosting voltage DC–DC converters, this MS-T converter has particular beneficial features. For example, compared to the KY converter whose voltage conversion ratio is one plus the duty cycle [6], the MS-T converter is capable of regulating output voltage under a wide range of input voltage and load variations. Compared to the S-T converter that includes four diodes and two inductors [7], the MS-T converter has fewer components and only includes three diodes and one inductor. Compared to the Zeta converter, the MS-T converter has negligible input current ripple so that an input filter is unnecessary. Thus, the MS-T converter is a good topology to obtain high voltage to obtain sufficient output power. Therefore, establishing the effective and general model for the MS-T converter is necessary to describe its real dynamic behaviors to provide effective guidance for control design.

However, to date, only a few studies on this subject have been found in the open literature. In [9], the MS-T converter and its basic circuit operation principles have been explored. The mathematical model of the MS-T converter has been derived, and its output voltage ripple and the boundary between continuous and discontinuous conduction modes have also been presented. In [10], the averaged and small signal models for this MS-T converter operating in continuous conduction mode (CCM) have been derived. Then, its transfer functions are established and analyzed. Nevertheless, all the derivations and analyses of small signal model in [10] are based on the particular assumption that the MS-T converter has only two modes in CCM and that the voltage across two capacitors are the same. Thus, the transfer functions in [10] are not sufficiently effective and general to describe the real

Manuscript received Sep. 9, 2016; accepted Apr. 18, 2017
Recommended for publication by Associate Editor Chun-An Cheng.
†Corresponding Author: eecjob@126.com
Tel: +86-29-82668630-218, Xi'an Jiaotong University
State Key Laboratory of Electrical Insulation and Power Equipment, School of Electrical Engineering, Xi'an Jiaotong University, China

characteristics of the MS-T converter if these particular assumptions are not satisfied. Accordingly, when the physical situation is fully considered, the improved transfer functions of the MS-T converter operating in CCM are derived and analyzed by establishing its improved average and small signal models. Then, based on the derived transfer functions, the voltage controller is applied for this MS-T converter.

The rest of the paper is organized as follows: in Section II, the circuit operations of the MS-T converter operating in CCM are briefly described and some insights are presented. In Section III, the improved average and small signal models of the MS-T converter that operate in CCM are established and its transfer functions are derived and analyzed. In Section IV, the voltage controller is applied for this MS-T converter. In Section V, the comparisons are presented to validate the effectiveness of the derived model. In Section VI, the circuit experimental results are provided for further validation. Finally, concluding comments are provided in Section VII.

## II. Circuit Operations and Some Insights

The MS-T converter is shown in Fig. 1. It consists of two power switches, $Q_1$ and $Q_2$; three diodes, $D_1$, $D_2$, and $D_3$; two capacitors, $C_1$ and $C_2$; one inductor $L$; one input voltage $v_{in}$; and one load $R_L$. Both two power switches ($Q_1$ and $Q_2$) that operate synchronically are controlled by the same PWM signal $v_d$ with the switching frequency being $f$ ($T$=1/$f$) and the duty cycle being $d$. The current through the inductor $L$ and capacitor $C_1$ are denoted by $i_L$ and $i_1$, respectively. The voltages across the capacitors ($C_1$ and $C_2$) are denoted by $v_{C1}$ and $v_0$, respectively. The components are assumed ideal.

The MS-T converter operating in CCM has three possible operational modes; that is, modes 1, 2, and 3, which are shown in Fig. 2.

Mode 1 (Fig. 2(a)) is described as two power switches ($Q_1$ and $Q_2$) that are turned on and three diodes ($D_1$, $D_2$, and $D_3$) that are turned off. Thus, the inductor $L$ is magnetized and both the capacitors ($C_1$ and $C_2$) are discharged so that voltages $v_{C1}$ and $v_0$ decrease. The corresponding equations for the MS-T converter operating in mode 1 can be established as follows:

$$\begin{cases} \dfrac{di_L}{dt} = \dfrac{v_{in} + v_{C1}}{L} \\ \dfrac{dv_0}{dt} = -\dfrac{v_0}{R_L C_2} \\ \dfrac{dv_{C1}}{dt} = -\dfrac{i_L}{C_1} \end{cases} \tag{1}$$

Mode 2 (Fig. 2(b)) is described as two power switches ($Q_1$ and $Q_2$) and diode $D_3$ that are turned off while the diodes $D_1$ and $D_2$ are turned on. Thus, the capacitor $C_1$ is charged by the input voltage $v_{in}$ together with the inductor $L$, and the capacitor $C_2$ remains discharged. Thereby, the voltage $v_{C1}$ increases, whereas the voltage $v_0$ decreases. The

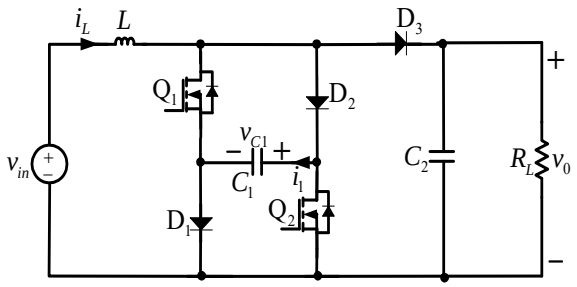


Fig. 1. Circuit schematic of MS-T converter.

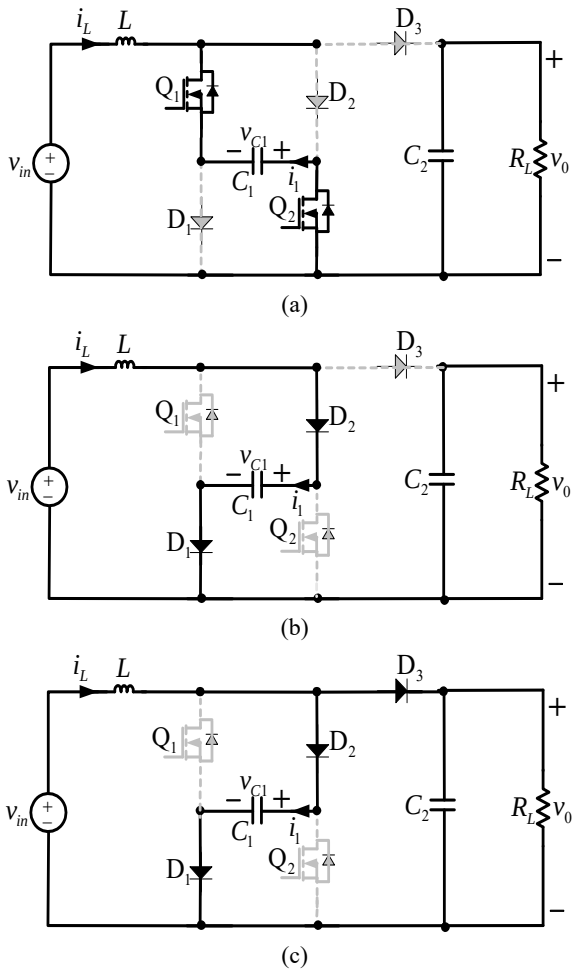


Fig. 2. Possible operational modes of MS-T converter operating in CCM. (a) Mode 1. (b) Mode 2. and (c) Mode 3.

corresponding equations for the MS-T converter that operates in mode 2 are given by

$$\begin{cases} \dfrac{di_L}{dt} = \dfrac{v_{in} - v_{C1}}{L} \\ \dfrac{dv_0}{dt} = -\dfrac{v_0}{R_L C_2} \\ \dfrac{dv_{C1}}{dt} = \dfrac{i_L}{C_1} \end{cases}. \tag{2}$$

Mode 3 (Fig. 2(c)) is denoted such that two power switches ($Q_1$ and $Q_2$) are turned off and three diodes ($D_1$, $D_2$, and $D_3$)

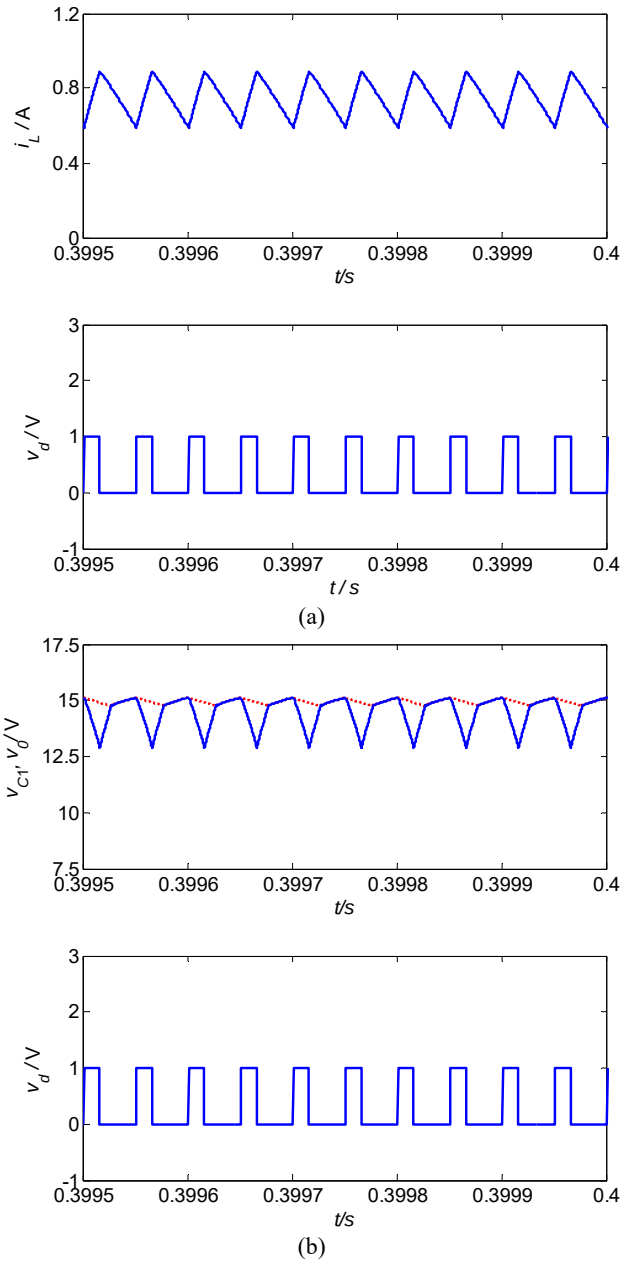


Fig. 3. PSIM simulated time-domain waveforms of the MS-T converter operating in CCM. (a) The inductor current $i_L$ and the PWM signal $v_d$. (b) The voltage $v_{C1}$ (solid line), the voltage $v_0$ (dashed line) and the PWM signal $v_d$.

are turned on. Thereby, both the capacitors $C_1$ and $C_2$ are charged by the input voltage $v_{in}$ together with the inductor $L$. The voltage $v_{C1}$ equals the voltage $v_0$. The model for the MS-T converter that operates in mode 3 can be expressed as follows:

$$\begin{cases} \dfrac{di_L}{dt} = \dfrac{v_{in} - v_0}{L} \\ \dfrac{dv_0}{dt} = \dfrac{i_L}{C_2} - \dfrac{i_1}{C_2} - \dfrac{v_0}{R_L C_2} \\ v_{C1} = v_0 \end{cases}. \tag{3}$$

Based on the PSIM software [11-12] and by choosing $v_{in}$=6V, $L$=1 mH, $C_1$=5 μF, $C_2$=22 μF, $R_L$=50 Ω, $f$=20 kHz, $T$=1/$f$, and $D$=0.3, the time-domain waveforms of the inductor current $i_L$ and the PWM signal $v_d$ of the MS-T converter operating in CCM are shown in Fig. 3(a), and its voltage $v_{C1}$, voltage $v_0$, and PWM signal $v_d$ are shown in Fig. 3(b). Figure 3 indicates that the MS-T converter has three modes and that the voltage $v_{C1}$ is not equal to the voltage $v_0$ in the entire switching period. However, the derivations and analyses of transfer functions of the MS-T converter operating in CCM in [10] are only suitable for the particular assumption that the MS-T converter operating in CCM has only two modes and the voltage $v_{C1}$ is equal to the voltage $v_0$ in the entire switching period. Thus, using the extant model in [10] to describe the real dynamical behaviors of the MS-T converter in other situations is difficult.

## III. Improved Transfer Functions

To establish the improved transfer functions of the MS-T converter operating in CCM, some symbols are first defined. $\langle x \rangle$ is the average value of $x$, where $x$ is the circuit variables, such as $i_L$, $i_1$, $v_{C1}$, $v_0$, $d$, $v_{in}$, $v_{vf}$, and $d_{11}$. $X$ is defined as the DC value of $\langle x \rangle$, and $\hat{x}$ is defined as its small ac value. Furthermore, the following equation is assumed:

$$\langle x \rangle = X + \hat{x} \quad \text{with} \quad \hat{x} << X \ . \tag{4}$$

As described in Section II, generally, the MS-T converter that operates in CCM has three modes: 1, 2, and 3. From equations (1), (2), and (3) and using the averaging method [13], the averaged model of the MS-T converter operating in CCM can be directly obtained as follows:

$$\begin{cases} \dfrac{d\langle i_L \rangle}{dt} = \dfrac{\langle v_{in} \rangle + \langle v_{C1} \rangle (d - d_{11}) - \langle v_0 \rangle (1 - d - d_{11})}{L} \\ \dfrac{d\langle v_0 \rangle}{dt} = (\dfrac{\langle i_L \rangle}{C_2} - \dfrac{\langle i_1 \rangle}{C_2})(1 - d - d_{11}) - \dfrac{\langle v_0 \rangle}{R_L C_2} \end{cases}. \tag{5}$$

Obviously, the items $\langle v_{C1} \rangle$, $\langle i_1 \rangle$, and $d_{11}$ in (5) lead these equations to be incomplete. In other words, deriving the expressions for these three items is necessary. To see the relationship between the voltage $v_0$ and voltage $v_{C1}$ clearly, the close-up view of Fig. 3(b) is presented and shown in Fig.4. Notably, the voltage $v_0$ and the voltage $v_{C1}$ are denoted by $V_{N11}$ at $NT$, $V_{N14}$ at $(N+1)T$, and $V_{N13}$ at $(N+d+d_{11})T$. $V_{N11}$=$V_{N14}$. The voltage $v_{C1}$ is denoted by $V_{N12}$ at $(N+d)T$. From (1), (2), (3) and Fig. 4, the following equations can be derived by using the geometrical technique:

$$V_{N11} - V_{N12} = \frac{\langle i_L \rangle}{C_1} dT \ , \tag{6}$$

$$V_{N13} - V_{N12} = \frac{\langle i_L \rangle}{C_1} d_{11} T \ , \tag{7}$$

$$V_{N11} - V_{N13} = \frac{\langle v_0 \rangle}{R_L C_2} (d + d_{11}) T \ . \tag{8}$$

Thus, the expression for $d_{11}$ can be derived by using (6)

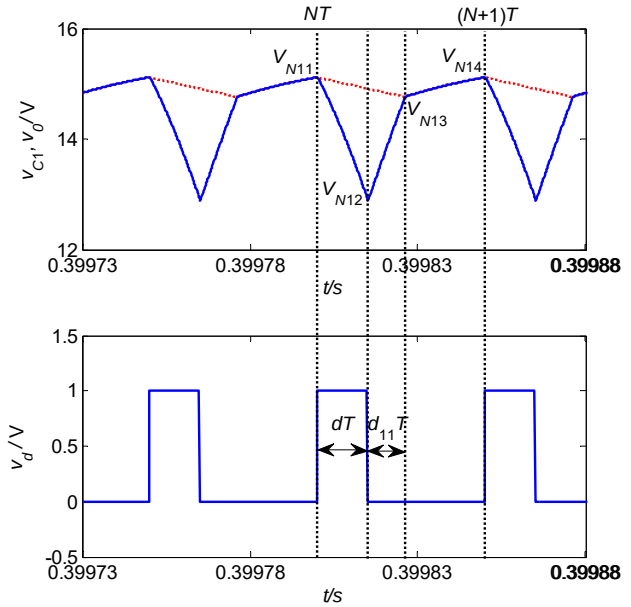


Fig. 4. Close-up view of voltage $v_{C1}$, voltage $v_0$, and PWM signal $v_d$.

minus the sum of (7) and (8).

$$d_{11}=\frac{R_LC_2\langle i_L\rangle-C_1\langle v_0\rangle}{R_LC_2\langle i_L\rangle+C_1\langle v_0\rangle}d \tag{9}$$

By using the geometrical technique and Fig. 4, the voltage $\langle v_0\rangle$ and the voltage $\langle v_{C1}\rangle$ can be given by

$$\langle v_0\rangle=\frac{V_{N11}+V_{N13}}{2}(d+d_{11})+\frac{V_{N13}+V_{N11}}{2}(1-d-d_{11}) \tag{10}$$

$$\langle v_{C1}\rangle=\frac{V_{N12}(d+d_{11})}{2}+\frac{V_{N13}(1-d)+V_{N11}(1-d_{11})}{2} \tag{11}$$

Consequently, the voltage $\langle v_{C1}\rangle$ can be derived by subtracting (11) from (10) and using (6), (7), and (9).

$$\langle v_{C1}\rangle=\langle v_0\rangle-\frac{R_LC_2\langle i_L\rangle^2-C_1\langle v_0\rangle\langle i_L\rangle}{(R_LC_2\langle i_L\rangle+C_1\langle v_0\rangle)C_1}d^2T \tag{12}$$

Besides, based on the ampere-second balance, $\langle i_1\rangle$ can be expressed as a function of $\langle i_L\rangle$, $d$ and $d_{11}$ to be

$$\langle i_1\rangle=\frac{d-d_{11}}{1-d-d_{11}}\langle i_L\rangle \tag{13}$$

By substituting (9), (12), and (13) into (5), the complete improved averaged model of the MS-T converter can be obtained as follows:

$$\begin{cases}\dfrac{d\langle i_L\rangle}{dt}=\dfrac{\langle v_{in}\rangle+\langle v_0\rangle(2d-1)}{L}-\dfrac{2\langle v_0\rangle\langle i_L\rangle(R_LC_2\langle i_L\rangle-C_1\langle v_0\rangle)d^3}{Lf(R_LC_2\langle i_L\rangle+C_1\langle v_0\rangle)^2}\\ \dfrac{d\langle v_0\rangle}{dt}=\dfrac{1}{C_2}(1-2d)\langle i_L\rangle-\dfrac{\langle v_0\rangle}{R_LC_2}\end{cases} \tag{14}$$

The DC equilibrium point of the MS-T converter operating in CCM can be obtained by substituting (4) into (9), (12), and (14), and then all small ac components are set as zero. The result is

$$D_{11}=\frac{C_2-C_1(1-2D)}{C_2+C_1(1-2D)}D \tag{15}$$

$$V_0=\frac{V_{in}R_L(C_2+C_1(1-2D))^2}{2D^3T(C_2-C_1(1-2D))+R_L(C_2+C_1(1-2D))^2(1-2D)} \tag{16}$$

$$I_L=\frac{V_{in}(C_2+C_1(1-2D))^2/(1-2D)}{2D^3T(C_2-C_1(1-2D))+R_L(C_2+C_1(1-2D))^2(1-2D)} \tag{17}$$

$$V_{C1}=\frac{V_{in}(C_1R_L(C_2+C_1(1-2D))^2-(C_2^2/(1-2D)-C_1^2(1-2D))D^2T)}{2C_1D^3T(C_2-C_1(1-2D))+R_LC_1(C_2+C_1(1-2D))^2(1-2D)} \tag{18}$$

From (16), (17), and (18), the voltage $V_0$, the inductor current $I_L$ and voltage $V_{C1}$ include not only the duty cycle $D$ and input voltage $V_{in}$, but also the two capacitors ($C_1$ and $C_2$), the switching period $T$, and the load $R_L$.

By taking (4) into (14) and then extracting the ac parts and neglecting the high-order small ac terms because their values are small, the small signal model of the MS-T converter operating in CCM can be given by

$$\begin{cases}\dfrac{d\hat{i}_L}{dt}=a_{11}\hat{i}_L+a_{12}\hat{v}_0+a_{13}\hat{d}+\dfrac{\hat{v}_{in}}{L}\\ \dfrac{d\hat{v}_0}{dt}=\dfrac{(1-2D)}{C_2}\hat{i}_L-\dfrac{1}{R_LC_2}\hat{v}_0-\dfrac{2I_L}{C_2}\hat{d}\end{cases}, \tag{19}$$

where

$$a_{11}=-\frac{2T(2R_LC_2V_0I_LD^3-C_1V_0^2D^3)}{L(R_LC_2I_L+C_1V_0)^2}$$

$$a_{12}=\frac{2D-1}{L}-\frac{2TR_LC_2I_L^2D^3-4TC_1I_LV_0D^3}{L(R_LC_2I_L+C_1V_0)^2}$$

$$a_{13}=\frac{2V_0}{L}-\frac{6TR_LC_2V_0I_L^2D^2-6TC_1V_0^2I_LD^2}{L(R_LC_2I_L+C_1V_0)^2}.$$

Then, the transfer functions including the input-to-output transfer function $G_{vv}(s)$, the control-to-output transfer function $G_{vd}(s)$, the input-to-inductor current transfer function $G_{iv}(s)$, and the control-to-inductor current transfer function $G_{id}(s)$ of the system can be derived by using Laplace transform on (19) and their respective definitions.

$$G_{vv}(s)=\frac{(1-2D)/L}{s^2C_2+s(G_L-a_{11}C_2)+a_{12}(2D-1)-G_La_{11}} \tag{20}$$

$$G_{vd}(s)=\frac{a_{13}(1-2D)+2I_La_{11}-2I_Ls}{s^2C_2+(G_L-C_2a_{11})s+a_{12}(2D-1)-G_La_{11}} \tag{21}$$

$$G_{iv}(s)=\frac{(sC_2+G_L)/L}{s^2C_2+s(G_L-a_{11}C_2)+(2D-1)a_{12}-a_{11}G_L} \tag{22}$$

$$G_{id}(s)=\frac{sa_{13}C_2+a_{13}G_L-2I_La_{12}}{s^2C_2+s(G_L-a_{11}C_2)+(2D-1)a_{12}-a_{11}G_L} \tag{23}$$

## IV. Closed-Loop Transfer Function

In this section, the voltage controller is applied to control the MS-T converter and its circuit schematic is shown in Fig. 5.

This circuit can be described by the following equation:

$$\frac{dd}{dt}=-\frac{d}{R_{vf}C_{vf}}-\frac{v_0}{V_mC_{vf}R_{vi}}+\left(\frac{1}{R_{vi}}+\frac{1}{R_{vd}}+\frac{1}{R_{vf}}\right)\frac{V_{ref}}{V_mC_{vf}}, \tag{24}$$

where $V_{ref}$ is the reference voltage and $V_m$ is the peak-to-peak

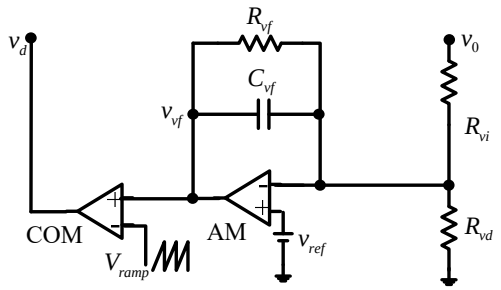


Fig. 5. Circuit schematic of voltage controller.

value of the ramp signal $V_{ramp}$.

By taking (4) into (24) and then separating the DC and small ac values, the following expressions can be obtained:

$$V_0 = (1+\frac{R_{vi}}{R_{vd}}+\frac{R_{vi}}{R_{vf}})V_{ref} - \frac{DV_m}{R_{vf}}R_{vi} \quad , \tag{25}$$

$$\hat{d}(s) = -H(s)\hat{v}_0(s) \quad , \tag{26}$$

where $H(s) = \dfrac{R_{vf}}{V_m R_{vi}(sR_{vf}C_{vf}+1)}$.

Accordingly, the closed-loop transfer function from the input to output can be derived by combining (16), (20), (21), (25), and (26).

$$G_{cvv}(s) = \frac{V_m R_{vi}(1-2D)(sR_{vf}C_{vf}+1)}{b_{11}s^3 + b_{12}s^2 + b_{13}s + b_{14}}, \tag{27}$$

where

$b_{11} = R_{vf}C_{vf}V_m R_{vi}LC_2$

$b_{12} = V_m R_{vi}LC_2 + R_{vf}C_{vf}V_m R_{vi}L(G_L - a_{11}C_2)$

$b_{13} = (a_{12}(2D-1) - G_L a_{11})R_{vf}C_{vf}V_m R_{vi}L + (G_L - a_{11}C_2)V_m R_{vi}L - 2I_L LR_{vf}$

$b_{14} = (a_{12}(2D-1) - G_L a_{11})V_m R_{vi}L + (a_{13}(1-2D) + 2I_L a_{11})LR_{vf}$

If all the poles of (27) are on the left side of the complex plane, the system is in stable operation.

## V. Comparisons

To validate the effectiveness of derivations preliminary, the derived models in this study and the existing models in [10] are calculated in theory and compared with the PSIM simulations in this section. Notably, the PSIM simulations on the bode diagram are obtained from the switch model of the MS-T converter, and not from its averaged model. Thus, it can be used to confirm the effectiveness of the derived transfer functions [11–12], preliminary.

### *A. Comparisons of DC Model in Open Loop*

From (17), the inductor current $I_L$ under different values of the input voltage $v_{in}$ can be calculated and shown in Fig. 6. Moreover, the corresponding DC values from the existing model [10] and from the PSIM simulations are also computed and plotted in Fig. 6. The results from the derived model in this study are more in good agreement with the PSIM simulations than those in [10].

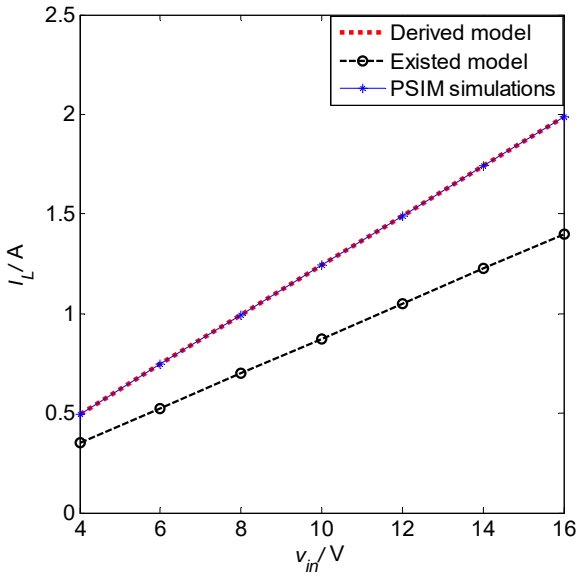


Fig. 6. Comparisons of inductor current $I_L$ among derived model, existing model in [10], and PSIM simulations.

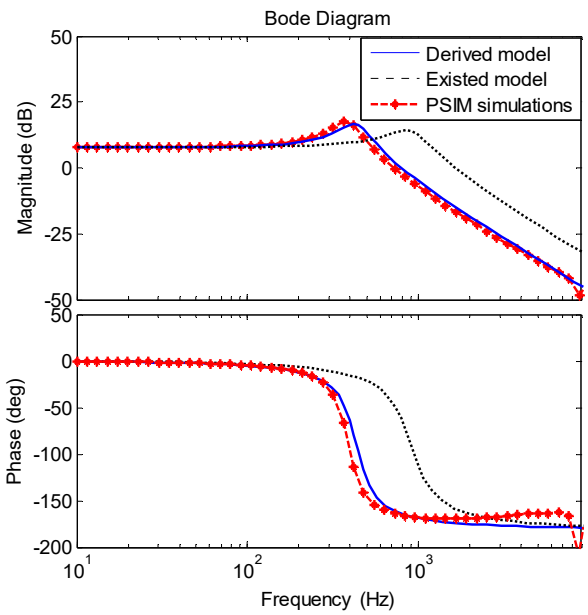


Fig. 7. Comparisons of input-to-output transfer function among the derived model, existing model in [10], and PSIM simulations.

### *B. Comparisons of Transfer Function in Open Loop*

As is well known, the precise transfer function of the system is useful in describing its small signal dynamical behaviors and providing a good guidance for control design. Thus, validating its effectiveness is necessary. In this study, only the input-to-output transfer function $G_{vv}(s)$ is chosen as an example to validate its effectiveness. The bode diagrams of $G_{vv}(s)$ and $G_{vv0}(s)$ (see Equation (40) in [10]) from the theoretical calculations and the PSIM simulations are shown in Fig. 7. The theoretical calculations about $G_{vv}(s)$ are more in good agreement with the PSIM simulations than $G_{vv0}(s)$ in [10].

TABLE I
POLES OF $G_{CVV}(s)$

| $C_{vf}$ | $\lambda_{1,2}$ | $\lambda_3$ | State |
|---|---|---|---|
| 1000nF | -395.1±2583.7i | -299.20 | Stable |
| 400nF | -232.2±2557.3i | -775.10 | Stable |
| 350nF | -193.9±2558.3i | -887.30 | Stable |
| 300nF | -144.5±2563.3i | -1033.8 | Stable |
| 250nF | -79.30±2576.4i | -1230.7 | Stable |
| 205nF | -1.800±2601.3i | -1473.6 | Stable |
| 204nF | 0.200±2602.1i | -1480.0 | Unstable |

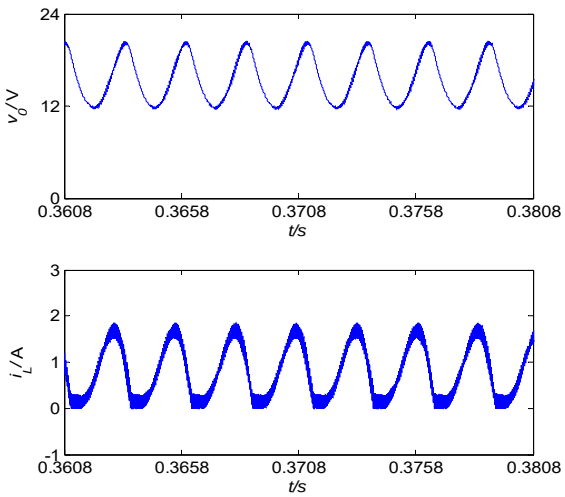


Fig. 8. PSIM simulated time-domain waveforms of voltage $v_0$ and inductor current $i_L$ under $C_{vf}$=100 nF.

### C. Comparisons of Identification on Stability

As is well known, the closed-loop transfer function can be used to identify the stability of the closed-loop controlled DC–DC converter. The circuit parameters for the voltage controller are chosen as $R_{vi}$=100 kΩ, $R_{vd}$=10 kΩ, $R_{vf}$=10 kΩ, $V_m$=4 V, $f$=20 kHz, and $V_{ref}$=1.3 V. From (27), the poles of the voltage controlled MS-T converter under different values of the capacitor $C_{vf}$ can be calculated and shown in Table 1. Obviously, if $C_{vf}$≧205 nF, the system is in stable operation. However, from the existing model in [10], the stable condition is $C_{vf}$≧75 nF. By taking $C_{vf}$=100 nF as an example, the PSIM simulations (Fig. 8) show that the system is indeed in unstable operation. Thus, the derived model in this study is more effective than the existing model in identifying the stability of the voltage-controlled MS-T converter.

## VI. CIRCUIT EXPERIMENTS

To further verify the effectiveness of the improved transfer functions, the hardware circuit for the MS-T converter with the voltage controller is designed and shown in Fig. 9. The power switches ($Q_1$ and $Q_2$) are realized by the HEXFET Power MOSFET IRFP064N, and the diodes ($D_1$, $D_2$, and $D_3$)

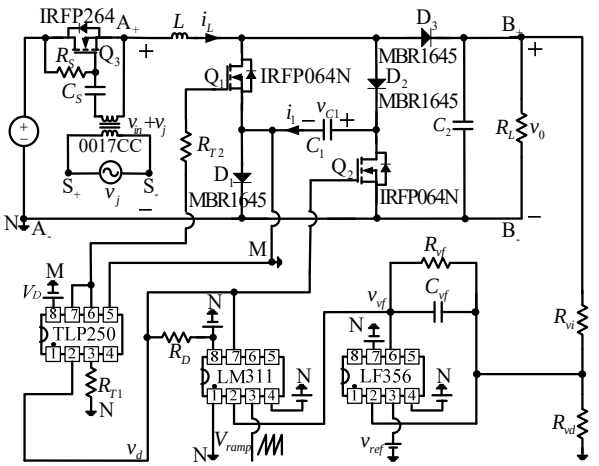


Fig. 9. Experimental circuit for voltage controlled MS-T converter.

are realized by the switch mode power rectifiers MBR1645. The digital oscilloscope GDS 3254 and impedance/gain-phase analyzer HP4194A are used to capture the measured time-domain waveforms and the measured gain and phase in the probes, respectively. The high voltage differential probes P5200A is applied to detect the voltages $v_{C1}$, the voltage $v_0$, and the PWM signal $v_d$ on the output of photocoupler TLP250 that generates the floating drive signal for the power switch $Q_1$.

In addition, to obtain the gain and phase of the input-to-output transfer function of the MS-T converter from the circuit experiments, the small signal source $v_j$ from the single terminal of the impedance/gain-phase analyzer HP4194A is injected into the input voltage [14]. Then, by the reference channel (RC) is used to detect the small signal source $v_j$ and the test channel (TC) to detect the small signal output voltage response. The circuit for the small signal source injection includes the electronic transformer 0017CC, the capacitor $C_S$=470μF, the resistor $R_S$=300Ω, and the HEXFET Power MOSFET IRFP264.

### A. Circuit Experiments in Open-Loop

Under the given circuit parameters in Section 2 and replacing the voltage controller by the PWM signal $v_d$ from the signal generator to make the MS-T converter operating in open loop, the inductor current $i_L$, voltages $v_{C1}$, voltage $v_0$, and PWM signal $v_d$ of the MS-T converter from the circuit experiments are shown in Fig. 10.

A comparison of Figs. 10 and 3 show that their averaged values are evidently in good agreement with each other. However, the detailed waveforms of Figs. 3(a) and 10(a) indicate a slight difference because in Fig. 3(a), the inductor current $i_L$ from the PSIM-simulated is obtained by assuming that all the circuit components are ideal so that its waveform is very clean. However, in Fig. 10(a), some undesired noise and waves are found in the waveform of the inductor current.


(a)


(b)

Fig. 10. Experimental time-domain waveforms (Time: 50 μs/div) for the MS-T converter in open-loop. (a) The inductor current $i_L$ (Top: 500 mA/div) and the PWM signal $v_d$ (Bottom: 10 V/div). (b) The voltage $v_0$ (Top: 2.5 V/div), the voltages $v_{C1}$ (Middle: 2.5 V/div), and the PWM signal $v_d$ (Bottom: 10 V/div).

These undesired noise and waves are mainly due to the non-ideal factor in the practical circuit, such as the on-resistor for the HEXFET Power MOSFET IRFP064N, especially the non-ideal drive signal that is generated from the photocoupler TLP250, among others. In addition, Fig. 10 further confirms that the three modes are in the MS-T converter operating CCM and that the voltage $v_{C1}$ is not equal to the voltage $v_0$ in the entire switching period.

Moreover, from the impedance/gain-phase analyzer HP4194A, the gain and phase of the input-to-output transfer function of the MS-T converter operating in CCM from the circuit experiments can be measured; these are shown in Fig.11.

Fig. 7 shows the theoretical calculations from the derived model here and the PSIM simulations about the gain and phase of bode diagram at 10 Hz is near 8 dB and 0 deg, respectively, and its peak gain occurs near 363 Hz. Fig. 11


(a)

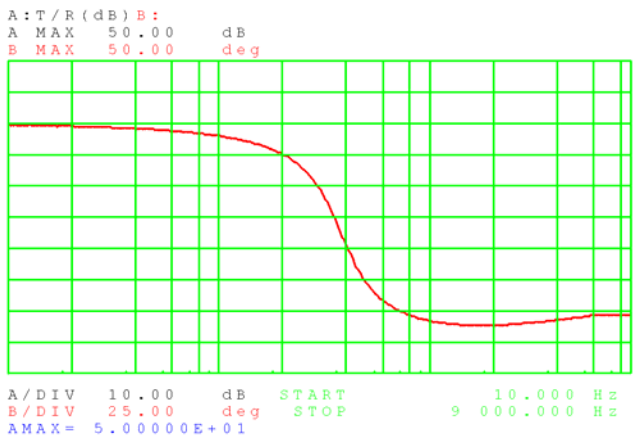


(b)

Fig. 11. Bode diagram of $G_{vv}$(s) from the circuit experiments (a) Gain, (b) Phase.

shows that the gain and phase of bode diagram at 10 Hz is near 7.9 dB and 0 deg, respectively, and its peak gain occurs at roughly 347 Hz. Accordingly, by comparing Fig.11 with Fig.7, the circuit experiments are in basic agreement with the theoretical calculations and the PSIM simulations. Therefore, the input-to-output transfer function here is an effective and general model for describing the real input-to-output characteristics of the MS-T converter operating in CCM.

### *B. Circuit Experiments in Closed-Loop*

Furthermore, under $C_{vf}$=100 nF, the circuit experimental results for the voltage controlled MS-T converter is shown in Fig.12. Figure 8 shows that roughly seven oscillation crests in the waveforms occur within 0.02 s and the peak output voltage $v_0$ and inductor current $i_L$ are 20.41 V and 1.845 A, respectively. Figure 12 clearly indicates that seven oscillation crests also occur in the waveforms within 0.02 s and the measured peak output voltage $v_0$ and inductor current $i_L$ are near 18 V and 1.8 A, respectively. Thus, Figs.8 and 12 are in basic agreement with each other. The slight difference between Figs. 8 and 12 is mainly caused by the parasitic

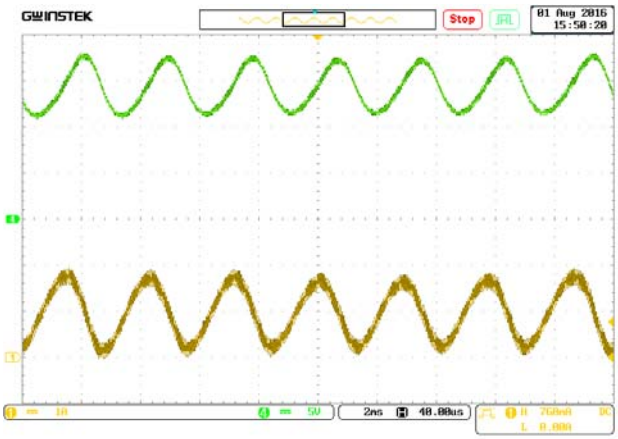


Fig. 12. Experimental time-domain waveforms (Time: 2 ms/div) of the voltage $v_0$ (Top: 5 V/div) and the inductor current $i_L$ (Bottom: 1 A/div) for the voltage controlled MS-T converter.

parameters in the experiments, especially the forward voltage drops on diodes. Thus, the derived model here is more effective and general than the existing ones for identifying the stability of the voltage controlled MS-T converter.

## VII. CONCLUSIONS

Based on the averaging method and by considering the relationship between the voltages across two capacitors, the improved averaged and small signal models of the MS-T converter operating in CCM are established. The DC equilibrium point and the transfer functions of the MS-T converter operating in CCM are derived and analyzed. The voltage controller is applied for the MS-T converter. Some comparisons among the derived model, the existing model in [10] and the PSIM simulations are presented. The theoretical calculations about the derived model here, the PSIM simulations, and the circuit experiments are in basic agreement with each other. All of them show that the improved transfer functions here are more effective and general than the existing ones for describing the real characteristics of the MS-T converter that operates in CCM. Therefore, one can apply the improved averaged and small signal model to design the MS-T converter and the corresponding controller to meet the requirements and targets of practical applications.

## ACKNOWLEDGMENT

Project supported by the National Natural Science Foundation of China (51377124 and 51521065) and the New Star of Youth Science and Technology of Shaanxi Province (2016KJXX-40).

## REFERENCES

[1] S. Ben-Yaakov and I. Zeltser, "The dynamics of a PWM boost converter with resistive input," *IEEE Trans. Ind. Electron.*, Vol. 46, No. 3, pp. 613-619, Jun. 1999.

[2] Y. Fuad, W. L. de Koning, and J. W. van der Woude, "On the stability of the pulsewidth-modulated Cuk converter," *IEEE Trans. Circuits Syst. II, Exp. Briefs*, Vol. 51, No. 8, pp. 412-420, Aug. 2004.

[3] V. Subramanian and S. Manimaran, "Implementation of a sliding mode controller for single ended primary inductor converter," *Journal of Power Electronics*, Vol. 15, No. 1, pp. 39-53, Jan. 2015.

[4] T. F. W and Y. K. Chen, "Modeling PWM DC/DC converters out of basic converter units," *IEEE Trans. Power Electron.*, Vol. 13, No. 5, pp. 870-881, Sep. 1998.

[5] F. L. Luo and H. Ye, "Positive output super-lift converters," *IEEE Trans. Power Electron.*, Vol. 18, No. 1, pp. 105-113, Jan. 2003.

[6] K. I. Hwu and Y. T. Yau, "KY converter and its derivatives," *IEEE Trans. Power Electron.*, Vol. 24, No. 1, pp. 128-137, Jan. 2009.

[7] E. H. Ismail, A. J. Sabzali, and M. A. Al-Saffar, "A high-quality rectifier based on Sheppard-Taylor converter operating in discontinuous capacitor voltage mode," *IEEE Trans. Ind. Electron.*, Vol. 55, No. 1, pp. 38-48, Jan. 2008.

[8] C. C. Hua, H. C. Chiang, and B. Y. Li, "Analysis and design of a novel Boost circuit originated in Sheppard-Taylor topology," in *6th IEEE Conference on Industrial Electronics Applications (ICIEA)*, pp. 1593-1598, Jun. 2011.

[9] C. C. Hua, H. C. Chiang, and C. W. Chuang, "New boost converter based on Sheppard-Taylor topology," *IET Power Electronics*, Vol. 7, No. 1, pp. 167-176, Jan. 2014.

[10] C. C. Hua, H. C. Chiang, and C. W. Chuang, "Small signal analysis of a new boost converter based on Sheppard-Taylor topology," *Journal of the Chinese Institute of Engineering*, Vol. 37, No. 3, pp. 346-357, 2014.

[11] PSIM User's Guide, Version 9.0, Release 3, Powersim Inc. May 2010.

[12] N. Femia, M. Fortunato, G. Petrone, G. Spagnuolo, and M. Vitelli, "Dynamic model of one-cycle control for converters operating in continuous and discontinuous conduction modes," *International Journal of Circuit Theory and Applications*, Vol. 37, pp. 661-684, May 2008.

[13] R. Middlebrook and S. Cuk, "A general unified approach to modelling switching-converter power stages," *International Journal of Electronics*, Vol. 42, No. 6, pp. 521-550, 1977.

[14] B. Swaminathan and V. Ramanarayanan, "Application of network analyzer in measuring the performance functions of power supply," *Journal of the Indian Institute of Science*, Vol. 86, No. 4, pp. 315-325, 2006.

**Faqiang Wang** was born in China in 1980. He received his B.S. in Automation from Xiangtan University, Xiangtan, China in 2003, and M.S. and Ph.D. in Electrical Engineering from Xi'an Jiaotong University, Xi'an, China in 2006 and 2009, respectively. From 2009 to 2011, he was a lecturer with the School of Electrical Engineering, Xi'an Jiaotong University. Since 2011, he has been an Associate Professor at the School of Electrical Engineering, Xi'an Jiaotong University. His current research interests include nonlinear dynamics and bifurcation analysis in power electronics.